Combustion and Flame 261 (2024) 113325

Contents lists available at ScienceDirect

Combustion and Flame

journal homepage: www.sciencedirect.com/journal/combustion-and-flame

An experimental, theoretical, and kinetic modeling study of post-flame oxidation of ammonia

Jie Jian [a], Hamid Hashemi [a], Hao Wu [a], Peter Glarborg [a,*], Ahren W. Jasper [b], Stephen J. Klippenstein [b]

[a] DTU Chemical Engineering, Technical University of Denmark, DK-2800 Lyngby, Denmark
[b] Chemical Sciences and Engineering Division, Argonne National Laboratory, Lemont, IL 60439, USA

ARTICLE INFO

Keywords:
NH_3 oxidation
Flow reactor
Theory
Kinetic modeling

ABSTRACT

The post-flame oxidation rate of ammonia was investigated in a novel atmospheric pressure flow reactor at temperatures of 1280 ± 16 K and as a function of residence time and mixture composition (1-10% O_2, dry and moist). The experimental results, as well as selected data from literature, were analyzed using an updated detailed chemical kinetic model. The medium temperature, very lean conditions enhance the importance of reactions of the nitroxyl (HNO) intermediate. High-level theory was used to calculate the rate constant for HNO + NH_2, indicating that this step is significantly faster than values used in literature. Furthermore, a trajectory based approach was used to determine collision efficiencies for selected bath gases for HNO + M. The experimental results show that the NH_3 oxidation rate increases with temperature and O_2 concentration, while the presence of water vapor slightly inhibits reaction. Formation of NO and N_2O was strongly promoted at higher levels of O_2. Modeling results agreed well with the measurements, except at the lowest level of O_2. The predicted oxidation rate of NH_3 was shown to result from a delicate balance between chain branching and terminating steps involving NH_2, H_2NO, and HNO. Recent theoretical work on reactions of these species by Klippenstein and coworkers and Stagni et al. was instrumental in improving modeling predictions. After initiation, NO reached a pseudo-steady-state level, where the pathways to NO were largely balanced by the NH_2 + NO reaction. Nitric oxide was partly oxidized to NO_2, with the NH_2 + NO_2 reaction responsible for most of the N_2O formation.

Novelty and significance statement: This study provides the first detailed kinetic analysis of the lean post-flame oxidation of ammonia, based on time-resolved flow reactor data in a novel reactor. In addition to the post-flame oxidation rate of ammonia, data for formation of NO and N_2O were compared with modeling predictions. The medium temperature, very lean conditions enhance the importance of reactions of the HNO and H_2NO intermediates. Inclusion in the model of results from recent high-level theoretical work, including present calculations for HNO + NH_2 and HNO + M, was crucial for capturing the observed behavior. It is argued that the post-initiation steady-state NH_3 oxidation rates constitute important data for model validation, along with ignition delays and laminar flame speeds.

1. Introduction

The development of technologies able to burn ammonia has been the focus of research studies since the 60's, and several reviews of the use of ammonia as a fuel have been published [1–8]. The challenges across combustion technologies are similar and include concerns of combustion properties and emission characteristics. Focus has mostly been on the long ignition delay times and low laminar flame speed. However, reactions in the burnout region are also crucial. The low oxidation rate may result in incomplete oxidation and slip of ammonia. Furthermore, N_2O formed in this zone is unlikely to decompose, allowing this strong greenhouse gas to be emitted.

To improve design and operation of engines burning ammonia, it is important to develop reliable kinetic models. Much of the earlier work on NH_3 oxidation chemistry is covered by recent reviews [4–7,9]. It is a very active field of research, and over the last few years results have been reported from premixed flames [10–13], shock tubes [14–19], rapid compression machines [20], jet-stirred reactors [21–24], and

* Corresponding author.
E-mail address: pgl@kt.dtu.dk (P. Glarborg).

https://doi.org/10.1016/j.combustflame.2024.113325
Received 27 August 2023; Received in revised form 4 January 2024; Accepted 15 January 2024
Available online 19 January 2024

flow reactors [17,25–27]. A large number of kinetic models for NH_3 oxidation have been reported, including recent studies from Glarborg and coworkers [9,28,29], Stagni et al. [25,30], Mei et al. [10,11], Shrestha et al. [31,32], and Sarathy and coworkers [33].

The most suitable experimental device to characterize the burnout chemistry is the flow reactor. A significant fraction of the experimental data on nitrogen chemistry in combustion is obtained in atmospheric pressure, laminar flow quartz reactors [9]. The flow reactor setup offers access to reaction conditions (temperature, pressure, reactant concentrations) not easily covered by other experimental techniques. However, as discussed by Dryer et al. [34], experiments must be interpreted with care. The plug flow assumption may break down as a result of axial and/or radial gradients in species, momentum, and/or temperature; non-idealities imposed by the reactor wall boundaries, such as surface reaction and/or heat transfer; or changes in chemical reaction time scales with extent of reaction, initial reactant concentrations, pressure, and reaction temperature. An added complexity for ammonia, compared with hydrocarbon fuels, is that NH_3 has a selectivity in oxidation, forming either NO, N_2O, or N_2.

In the case of ammonia as a reactant, interference from reactions on the reactor surface is a particular concern, even for fairly inert materials such as quartz and alumina. Heterogeneous reactions may involve decomposition or oxidation of fuel components, promoting reaction, or loss of radicals, inhibiting reaction. Ammonia is known to decompose on quartz surfaces [35–37]. Stephens and Pease [38] reported similar degrees of oxidation of ammonia in filled and empty quartz reactors, but did find an effect of surface coating. Dean et al. [39] observed that heterogeneous effects affected induction times for oxidation of ammonia under conditions with large excess of O_2. For Thermal $DeNO_x$, where the initiation chemistry is not rate limiting due to the fast NH_2 + NO reaction, surface reactions are believed to be insignificant in low surface/volume quartz reactors [9,37,40].

Among the flow reactor studies reported for conditions relevant to the burnout region (significant excess of O_2) [39,41–44], only the data of Dean et al. [39] and Duo [41] were obtained as a function of reaction time, allowing a separation of the induction period and the post-initiation oxidation rate. In the present work, an experimental, theoretical, and kinetic modeling study of the post-flame oxidation rate of ammonia is conducted. Data are obtained in a novel atmospheric pressure flow reactor as a function of residence time, temperature, and mixture composition. By measuring the oxidation rate of ammonia after onset of reaction, surface interference is minimized. The present data, as well as the results of Dean et al. [39] and Duo [41], are analyzed using a detailed chemical kinetic model, drawn mostly from Glarborg et al. [9], but updated according to recent work. The medium temperature, very lean conditions representative of the burnout region enhance the importance of reactions of the nitroxyl (HNO) intermediate, and we apply high-level theory to calculate the rate constant for HNO + NH_2 and use a trajectory based approach to determine collision efficiencies for selected bath gases for HNO + M.

2. Experimental

2.1. Characteristics of the laminar flow reactor

As discussed above, data from flow reactors are prone to uncertainties in initial conditions, either due to conditioning (mixing, preheating) or interference from reactions on the reactor surface, even for fairly inert materials such as quartz and alumina. Other concerns include breakdown of the plug flow assumption, uncertainties in temperature profiles, etc. The impact of the uncertainties depends on reactant composition, reaction conditions, and reactor design. Two types of reactor designs can be identified:

Type I Premixed gases flow through a heated tube and undergo the temperature profile of the oven. Type I reactors operate in the laminar flow regime. Results on ammonia oxidation in Type I reactors have been presented by Kasaoka and coworkers [45–47], Dean et al. [39], Monnery et al. [48], Stagni et al. [25], and Zhu et al. [17] at atmospheric pressure, and by Song et al. [44] and Garcia-Ruiz et al. [27] at high pressure.

Type II Reactive gases are heated separately and mixed at the reactor inlet. This reactor type is designed for either turbulent or laminar flow. Results on ammonia oxidation are restricted to non-premixed reactors working in the laminar flow regime [26,38,41–43].

Dean et al. [39] conducted experiments in a type I laminar flow reactor under lean conditions. By varying reactor size and flow rate, they could observe the NH_3 decay and the NO formation as functions of reaction time. They investigated the impact of heterogeneous reactions by varying the surface to volume ratio (4–20 cm^{-1}) and the pretreatment of the quartz surface (fresh, extensive service, or washed with chromic-sulfuric acid). They observed significant variations in the induction time due to surface effects but no influence on either the post induction time NH_3 decay rate or on the NO production rate. The findings of Dean et al. may to some extent be specific for the type I reactor and the chosen reactant concentration range and temperature interval in their experiments. However, it is likely that the issue with the surface influence on induction time is relevant also for type II laminar flow reactors.

The advantage of the type II reactor is that the reaction zone is isothermal and the residence time at the set temperature is well defined. However, to be heated separately, the gases enter the reactor unmixed and the mixing region becomes important at high reaction rates. Mixing occurs primarily by molecular diffusion (laminar flow conditions), with typical mixing times of about 5 ms [49]. In the mixing region in type II reactors, there can locally be high concentrations of reactants as well as high S/V ratios, and it is conceivable that the induction time in NH_3 oxidation may be affected, similar to what has been reported for type I [39].

Artifacts of the laminar flow reactor can thus be expected to affect initiation of ammonia oxidation in quartz reactors of both type I and II. For this reason, it is important to decouple the induction period in the interpretation of the experimental results, as done commonly for the turbulent flow type II reactor [34]. This can only be achieved by obtaining time dependent or spatially resolved concentration profiles. To our knowledge, only Dean et al. [39] and Monnery et al. [48] in type I reactors and Duo [41] in a type II reactor have reported such data for oxidation of ammonia. The results from Dean et al. and Duo were obtained under relevant conditions and are included in the present analysis.

2.2. The variable-length flow reactor

In the present work, ammonia oxidation data were obtained in a modified type II reactor. A variable-length reactor (VLR) made of quartz was designed and used for the experiments. It was coupled with a three-zone electrically heated oven, as shown in Fig. 1. The reactor consisted of three parts: a reactor tube, a casing and an inlet tube. Ammonia diluted in N_2 entered the reactor through the inlet tube while the bulk flow, consisting of O_2 and H_2O with N_2 for balance, entered the reactor from the casing. The inlet tube could be moved along the axial length of the reaction tube. Thereby, the length of the reaction zone was adjustable, enabling the residence time to be varied in the range 50–250 ms and allowing for direct detection of the reaction rate after initiation.

The outlet of the reactor was connected to an FTIR (MGS300 MKS Instrument) for measuring NH_3, NO, N_2O, and H_2O concentrations. The

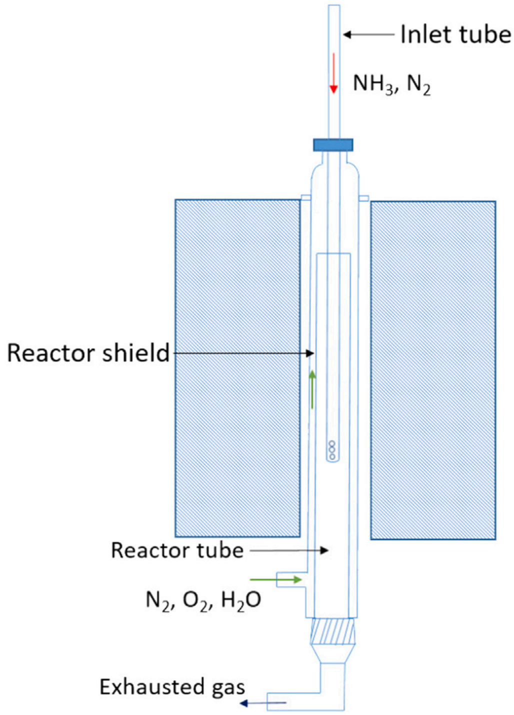

Fig. 1. Schematic overview of the variable-length reactor (VLR).

FTIR was calibrated for ammonia in the range 20–2000 ppm, and for NO from 9 to 450 ppm. The detection limits for NO and N_2O were 0.5 and 0.1 ppm, respectively, and the uncertainty was less than 10%. While most results were obtained from the VLR, selected reference experiments were performed in a conventional premixed reactor (PR), i.e., a straight quartz tube. The residence time for the experiments in the PR was varied by changing the flow rate.

2.3. Reactor temperature

In the ideal type II reactor, all reactants are preheated to the temperature of the isothermal zone prior to mixing. Unfortunately, this was not possible in the current reactor, where reaction could occur at temperatures below the set value, both in the inlet and exit sections. For this reason, the temperature profile was carefully evaluated. For each setting, it was measured by a K-type thermocouple. Thermocouples, especially with an oxidized casing, are known to readily absorb radiation, while gases, especially nitrogen or air, have poor radiation absorption ability. The contribution from radiative heat transfer results in an overestimation of the gas temperature in the preheating zone, as the thermocouple is heated directly by radiation from the heating elements.

To correct for the error in the measured temperature profiles, computational fluid dynamics (CFD) calculations using Ansys Fluent were used to estimate the actual gas temperature and determine a region in the reactor with a relatively constant temperature. Details are given in the Supplementary Material (SM). The thermocouple measurements are compared with CFD predictions in Fig. 2. The measured temperatures indicate an isothermal zone from 15 to 45 cm. However, according to the calculations, there is a considerable delay in the heating of the gas. From 10 to 30 cm, the predicted temperature increases by around 40 K, and the measurement error is significant. From 30 to 52 cm, the calculated variation in temperature is within 10 K. Accordingly, this region is taken as the isothermal zone. Reaction is assumed to be immediately quenched after 52 cm. According to modeling, this assumption introduces an error in NH_3 of less than 20 ppm. However, the ±10 K uncertainty in the temperature introduces an uncertainty in the predicted NH_3 oxidation rate ($d(X_{NH3}/X_{NH3i})/dt$) of about 20%.

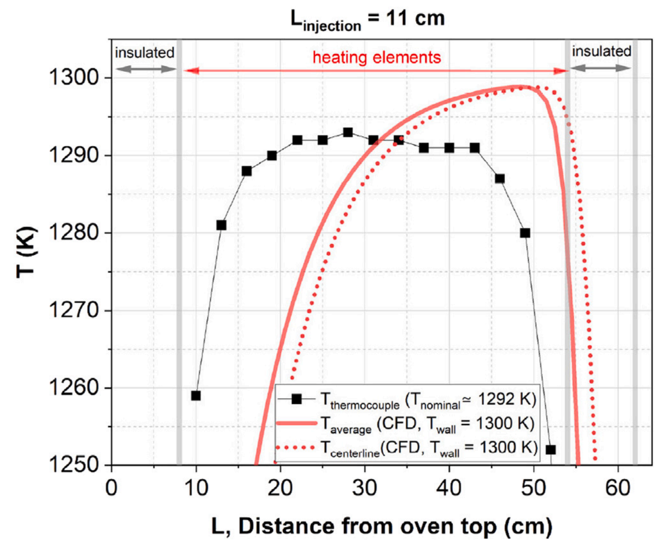

Fig. 2. Comparison of measured and calculated temperature profiles in the reactor tube along the oven height. The calculated temperature profile was obtained from CFD simulations.

3. Theory

The oxidation rate of NH_3 in the burnout region is sensitive to the production of chain carriers. Nitroxyl is an important intermediate, and the reactions of HNO affect the chain branching. At high temperatures, HNO dissociates rapidly. However, in the temperature range 1200–1300 K of interest in the present study, dissociation competes with HNO + O_2, as well as with reactions of HNO with the radical pool, in particular HNO + NH_2. In this section, we apply high-level theory to calculate the rate constant for HNO + NH_2 and use a trajectory based approach to determine relative collision efficiencies for selected bath gases for HNO + M.

3.1. HNO + NH_2

There appear to be only two prior theoretical studies of the HNO + NH_2 reaction. Mebel and coworkers obtained ab initio variational transition state theory (VTST) predictions for the direct abstraction to form NH_2 + NO and the related reverse reaction [50]. Their analysis was based on G2 theory, which employs MP2/6-311G(d,p) geometry optimizations and frequency evaluations. A follow up analysis by Xu and Lin provided a more extensive exploration of the potential energy surface (PES) and corresponding kinetics [51]. They considered the addition of NH_2 to both the N and O atoms of HNO together with the subsequent isomerizations and dissociations to a range of products. Their ab initio VTST kinetics predictions were based on CCSD(T)/6-311+G(3df,2p) // CCSD/6 311++G(d,p) evaluations.

The experimental data for this reaction are also very limited. Roose et al. studied the reverse reaction as part of a shock tube study of the decomposition of NO in the presence of ammonia [52,53]. Meanwhile, Glarborg et al. [37] examined its significance in a study of the Thermal de-NO_x process in flow reactors. Neither of these experiment/modeling based estimates are particularly direct, while the theoretical studies contain significant uncertainties (i.e., a few kcal/mol) in the barrier heights. Thus, it is perhaps not surprising that the estimates from theory and experiment differ by orders of magnitude. Advances in theory allow for much more accurate theoretical predictions, which we pursue here.

3.1.1. PES methodology

Our analysis builds from that of Xu and Lin [51] with significantly higher accuracy electronic structure predictions for the properties of the stationary points and for the key minimum energy paths. In particular, we obtain the geometries and vibrational frequencies for each of the kinetically relevant points on the NH_2 + HNO potential energy surface at the CCSD(T)-F12/cc-pVTZ-F12 level of theory. The minimum energy paths were evaluated at the same level of theory. A high-level composite approach was used to improve the accuracy of the key stationary point energies. This composite approach is analogous to the ANL0 method [54], with the main difference being the use of the more accurate CCSD(T)-F12/cc-pVTZ-F12 method in the vibrational analysis.

To be precise, the present ANL0′ composite energies consist of a CCSD(T)-F12/CBS-F12(TZF,QZF) energy (from explicit cc-pVTZ-F12 and cc-pVQZ-F12 energies), a CCSDT(Q)/cc-pVDZ correction for higher order excitations, a CCSD(T)/CBS(TZ,QZ) correction for core-valence interactions (based on extrapolation of data obtained for the cc-pcVTZ and cc-pcVQZ basis sets), a CCSD(T) relativistic correction, a HF/cc-pVTZ diagonal Born Oppenheimer correction (DBOC), CCSD(T)-F12/CBS-F12(DZF,TZF) harmonic zero point energies (ZPE) and B2PLYP-D3/cc-pVTZ anharmonic ZPE corrections. At this level of theory, 2σ uncertainties of ~0.2 kcal/mol are expected, unless the corrections for higher order excitations are larger than about 1 kcal/mol [54]. In contrast, the 2σ error bars from the prior theoretical analyses [50,51] are likely 2–3 kcal/mol at best.

3.1.2. Kinetics methodology

Predictions for the temperature and pressure dependence of the rate constants are obtained from transition state theory based master equation calculations incorporating the ab initio calculated properties of the requisite stationary points. Rigid-rotor harmonic oscillator (RRHO) state counts were supplemented with 1-dimensional hindered rotor torsional mode treatments and asymmetric Eckart tunneling corrections. The hindered rotor potentials were evaluated at the CCSD(T)/cc-pVTZ level. The collisional energy dependence of the energy transfer probabilities are represented with a temperature dependent exponential down form. The room temperature average downwards energy transfer parameter is set to 100 cm^{-1}, with a temperature dependence proportional to $T^{0.85}$, which are typical of small molecules colliding with N_2.

Variational effects were included for the key channels (i.e., for the NH_2 + HNO = NH_2…HNO, NH_2…HNO = NH_2NHO, and NH_2…HNO = NH_3…NO channels). The flux to form the NH_2…HNO van der Waals complex from the reactants was evaluated with variable reaction coordinate TST [55], employing a center-of-mass reaction coordinate. The orientation dependent interaction energies for these VRC-TST calculations were evaluated at the CCSD(T)-F12/cc-pVDZ-F12 level. The variational treatments for the NH_2…HNO = NH_2NHO, and NH_2…HNO = NH_3…NO channels employed reaction path methodologies with RRHO representations for the orthogonal modes.

Corrections for vibrational anharmonicity were included through the use of anharmonic fundamental frequencies within the RRHO expressions. At higher temperatures (i.e., above about 1000 K) such a fundamental frequency based approach begins to fail due to higher vibrational excitations. Nevertheless, the effect of such failures should largely be cancelled in the computation of the reaction rates, which involve ratios of transition state and reactant partition functions. For a few of the modes (i.e., the lowest two modes in the NH_2…NO = NH_3…NO transition state, and the lowest mode in the NH_2…NO = NH_2NHO transition state) the perturbative anharmonic vibration analysis appears to fail, as evidenced by overly large anharmonic corrections. In those cases, we simply employ the harmonic frequencies.

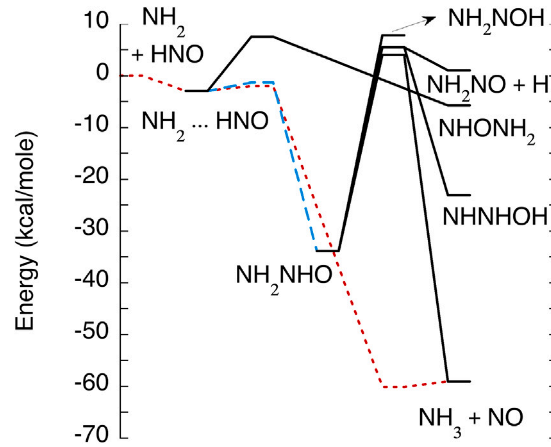

Fig. 3. Schematic diagram of the PES illustrating the primary reaction pathways for the reaction of NH_2 with HNO. The red dotted and blue dashed lines denote the two primary reaction channels yielding NH_3 + NO and NH_2NHO. All other channels are predicted to have a maximum branching below 1%.

3.1.3. Software used

The coupled cluster calculations were performed with the MOLPRO software [56], except for the DBOC corrections, which were obtained with CFOUR [57]. The MRCC module from Kallay [58,59] was used within MOLPRO to obtain the CCSDT(Q) corrections. Meanwhile, the B2PLYP-D3 density functional theory calculations were performed with Gaussian [60]. The VRC-TST calculations were performed with the VaReCoF program [61], while the master equation calculations were performed with the MESS master equation system solver [62,63]. The input file for the master equation calculations is provided as Supplementary Material.

3.1.4. Results

The components of the present ANL0′ composite calculations for the key reaction pathways in the NH_2 + HNO reaction are reported in Table 1. A corresponding schematic diagram is provided in Fig. 3. The ANL0′ predictions are compared with available literature data in Table 2.

The saddle points for the addition of NH_2 to the O end of HNO and for the conversion of NH_2NHO into NH_3 + NO have large T1 diagnostics and CCSDT(Q)/cc-pVDZ corrections, which are indicative of likely multireference effects. Fortunately, the master equation calculations indicate that these two channels do not contribute significantly to the reactive flux. Thus, an uncertainty of one or two kcal/mol for these channels is acceptable. Notably, all other stationary points should be reasonably well described by single reference based methods such as the ANL0′ method.

The active thermochemical tables (ATcT) values for the molecular species provide a useful benchmark for the accuracy of the ANL0′. As seen from Table 2, aside from NH_2NO + H, the maximum discrepancy between the ANL0′ and ATcT values is 0.25 kcal/mol for NNH + H_2O. The larger discrepancy of 0.50 kcal/mol for NH_2NO + H may be a result of a strong anharmonicity for the umbrella mode that is not well captured at the B2PLYPD3 level. Alternatively, the discrepancy may be indicative of a limitation in the ATcT value, which is largely based on a considerable number of lower level theoretical calculations such as Gn calculations. In any case, this species is not particularly relevant to the kinetics as the 5.5 kcal/mol barrier to its formation effectively precludes its formation.

The root mean square deviation between the values from Xu and Lin and the present ANL0′ values is 3.5 kcal/mol. This large value might be expected to lead to significant discrepancies between kinetics predictions based on the different sets of energetics. However, it is

Table 1
Components of stationary point energies (kcal/mol).

Stationary point	CCSD(T)-F12			T(Q)	CV	Rel.	DBOC	E0		Total[a]	T1[b]
	TZ-F12	QZ-F12	CBS	DZ	CBS	HF/TZ	RRHO		Anh		
NH_2 + HNO	0	0	0	0		0	0	0	0	0.0	0.016
NH_2…HNO	−4.51	−4.53	−4.53	−0.02	−0.04	0.02	−0.06	1.84	−0.16	−2.96	0.014
NH_3…NO	−63.34	−63.44	−63.48	0.00	−0.33	0.02	−0.06	4.07	−0.18	−60.14	0.017
NH_3 + NO	−61.97	−62.06	−62.11	0.02	−0.33	0.01	−0.05	3.58	−0.04	−59.08	0.021
NH_2…HNO = NH_3…NO	−2.43	−2.43	−2.43	−0.33	−0.01	0.01	0.04	0.99	−0.27	−2.00	0.027
NH_2…HNO = NH_2NHO	−1.99	−2.04	−2.06	−1.18	0.00	0.02		2.35	−0.43	−1.30	0.022
NH_2…HNO = NHONH_2	6.19	6.19	6.18	−2.26	0.09	0.00	0.06	3.52	−0.10	7.50	0.049
NH_2NHO = NH_3 + NO	3.62	3.56	3.53	−1.84	−0.12	0.06	−0.03	2.80	−0.42	3.99	0.039
NH_2NHO = NH_2NO + H	5.91	5.76	5.68	−0.79	−0.36	0.15	−0.07	1.05	−0.19	5.47	0.028
NH_2NHO = NHNHOH	2.48	2.20	2.06	−0.23	−0.39	0.20	−0.10	4.08	−0.10	5.53	0.027
NH_2NHO = NH_2NOH	4.93	4.69	4.57	−0.21	−0.24	0.12	−0.09	3.69	−0.07	7.78	0.021
NH_2NHO	−40.46	−40.72	−40.85	0.24	−0.56	0.26	−0.21	7.44	−0.58	−33.91	0.025
NH_2N + OH	9.65	9.55	9.51	0.35	−0.29	0.07	0.10	1.63	0.01	1.07	0.022
NHONH_2	−11.82	−12.04	−12.15	0.07	−0.10	0.11	−0.18	6.64	−0.12	−5.74	0.023
NHNOH + H	1.27	1.18	1.14	−0.07	−0.20	0.09	−0.19	0.30	0.00	1.07	0.017
NH_2NO + H	2.19	2.08	2.02	−0.21	−0.40	0.14	−0.20	−0.34		1.02	0.020
NHNHOH	−28.73	−29.01	−29.15	0.17	−0.42	0.04	−0.21	6.66	−0.14	−23.05	0.021
NNH + H_2O	−68.92	−69.06	−69.13	0.08	−0.43	0.09	−0.09	1.08	−0.11	−68.51	0.028
NHNH + OH	−15.36	−15.33	−15.31	0.32	−0.17	0.02	−0.12	2.41	0.05	−12.91	0.012

[a] The total includes experimental spin–orbit splittings for NO and OH in addition to the sum of the CCSD(T)-F12 CBS limit and the other energy components presented in the Table.
[b] T1 denotes the T1 diagnostic, which provides some indication of the extent of multireference effects.

Table 2
Comparison of ZPE corrected stationary point energies (kcal/mol) with literature values.

Stationary point	Mebel et al.[a] G2	Xu and Lin[b] CCSD(T) 6-311++G(3df,2pd)	Current[c] ANL′	ATcT[d]
NH_2 + HNO	0.0	0.0	0.0	0.0
NH_2…HNO	−2.3	−2.1	−2.96	
NH_3…NO			−60.14	
NH_3 + NO	−57.5	−57.8	−59.08	−58.97 ± 0.04
NH_2…HNO = NH_3…NO		−1.9	−2.00	
NH_2…HNO = NH_2NHO		No saddle point	−1.30	
NH_2…HNO = NHONH_2		11.0	7.50	
NH_2NHO = NH_3…NO		8.5	3.99	
NH_2NHO = NH_2NO + H		No saddle point	5.47	
NH_2NHO = NHNHOH		11.4	5.53	
NH_2NHO = NH_2NOH			7.78	
NH_2NOH = NHNOH + H		No saddle point		
NH_2NHO		−25.9	−33.91	
NH_2N + OH		12.3	11.07	10.99 ± 0.16
NHONH_2		−3.9	−5.74	
NHNOH + H		2.3	1.07	
NH_2NO + H		2.6	1.02	0.52 ± 0.23
NHNHOH		−22.1	−23.05	
NNH + H_2O		−65.6	−68.51	−68.26 ± 0.11
NHNH + OH		−12.0	−12.91	−13.02 ± 0.10
RMSD[e]		3.5		

[a] G2//MP2/6-311G(d,p) results from Mebel et al. [50].
[b] CCSD(T)/6-311++G(3df,2pd)//CCSD/6 311++G(d,p) results from Xu and Lin [51].
[c] Current best estimates from Table 1.
[d] Values from v1.124 of Active Thermochemical Tables accessed on June 20, 2023. https://atct.anl.gov/Thermochemical%20Data/version%201.124/index.php.
[e] Root-mean-square deviation of results from Xu and Lin [51] from current best estimates.

worth noting that for the most important saddle point (for NH_2…HNO = NH_3…NO) the discrepancy is only 0.1 kcal/mol.

The temperature dependence of the present predictions for the NH_2 + HNO → NH_3 + NO rate constant is illustrated in Fig. 4 together with the data from the literature. The master equation calculations indicate that this rate constant is effectively pressure independent below 100 atm. It is well represented by the expression $8.8 \times 10^6\ T^{2.00}\ \exp(1555/RT) + 6.7 \times 10^{16}\ T^{-1.407}\ \exp(-5/RT)$ $cm^3\ mole^{-1}\ s^{-1}$ over the 300 to 3000 K temperature range. It is not clear why the present predictions deviate so strongly (i.e., by about an order of magnitude) from those of Xu and Lin [51]. As noted above, the barrier energies for the primary channel differ by only 0.1 kcal/mol. Mebel et al. [50] and Xu and Lin have previously indicated shortcomings in the experimental reaction enthalpies employed in the analysis of Roose et al. [52,53].

Table 3
Modified Arrhenius representations of the pressure dependent rate constants in the NH_2 + HNO reaction system. Parameters for use in the modified Arrhenius expression $k = AT^{\beta}\exp(-E/[RT])$.

Reaction	Pressure (bar)	A (cm^3 $mole^{-1}$ s^{-1} or s^{-1})	β	E (cal/mole)
NH_2 + HNO = NH_2NHO	0.1	4.43E30	−6.70	3440
	0.3	8.56E30	−6.64	3810
	1	4.59E30	−6.39	4120
	3	1.17E30	−6.06	4360
	10	1.26E29	−5.61	4580
	30	2.45E27	−4.97	4460
	100	3.92E24	−4.00	3920
NH_2NHO = NH_3 + NO	0.1	1.47E39	−8.69	38 790
	0.3	2.06E37	−8.35	38 710
	1	1.05E36	−7.85	38 600
	3	1.50E34	−7.19	38 340
	10	4.47E31	−6.30	37 940
	30	9.67E28	−5.37	37 480
	100	2.87E25	−4.18	36 730

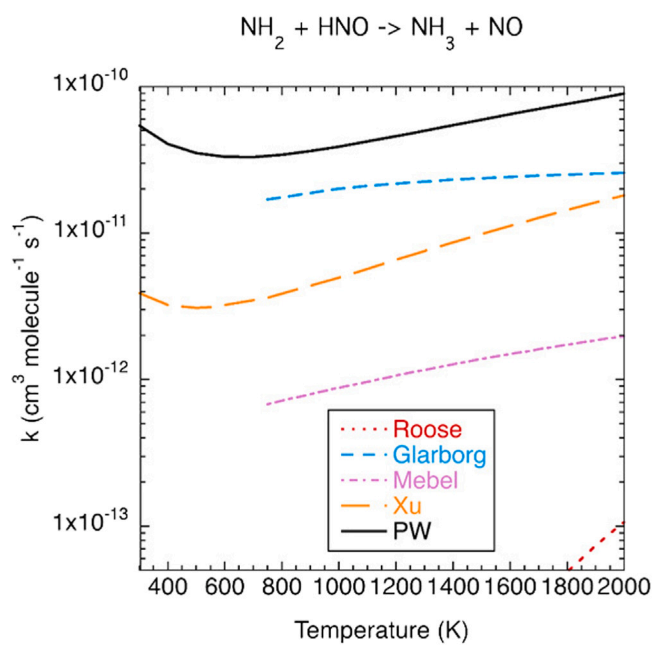

Fig. 4. Comparison of present predictions (PW) of the temperature dependence of the rate constant for the NH_2 + HNO → NH_3 + NO (R23) with literature data from prior theoretical (Mebel et al. [50], Xu and Lin [51]), experimental (Roose et al. [53]), and modeling (Glarborg et al. [37]) studies.

Remarkably, the empirical modeling result of Glarborg et al. [37] actually shows the best agreement with these predictions.

The rate constants for formation of NH_2NHO and decomposition of NH_2NHO into NH_3 + NO are strongly dependent on pressure. Modified Arrhenius representations of these rate constants are provided in Table 3 for a variety of pressures. These fits are valid over the 400 to 1600 K temperature range. Under the present conditions with atmospheric pressure and comparatively high temperature, formation of NH_2NHO cannot compete with the direct abstraction reaction, but for modeling of high pressure ignition delay times, this component should be taken into account.

3.2. HNO (+M)

The H + NO recombination reaction,

$$H + NO(+M) \rightleftharpoons HNO(+M) \quad (R17)$$

has only been measured directly at low temperature and only in the forward direction. Data for the H + NO + H_2 reaction, which is the most extensively studied [64–72], cover temperatures from 230 to 700 K, even though most results are obtained at room temperature. Results for other collision partners are scarce. For Ar, three low temperature studies have been reported [66,68,73], while Riley et al. [74] studied the H + NO + Ar reaction at 300–900 K.

The collision partners of greatest practical importance are N_2, H_2O, and NH_3. A single study [66] reports the collision efficiency of H_2O compared to Ar and H_2 at room temperature, while no data are available for HNO + NH_3. For the H + NO + N_2 reaction rate, only indirect determinations are available. Campbell and Handy [73] derived a rate constant at 392 K from a discharge-flow/stirred-reactor study of the O/H_2/NO system. Allen et al. [75] estimated a rate constant at 995 K, based on flow reactor results for the N_2O/H_2 system. Glarborg et al. [76] determined the rate constant for the H + NO + N_2 reaction in the temperature range 1000–1170 K from flow reactor experiments with addition of NO to $CO/O_2/H_2O$ strongly diluted in N_2. They also obtained a value of k_{17} at 2000 K from re-interpretation of results from a laminar premixed flame with a $H_2/O_2/NO/N_2$ mixture. More recently, Riley et al. [74] studied the H + NO + Ar reaction at 300–900 K.

To reconcile the results and to extrapolate to other gas mixtures, it is required to determine the relative efficiencies of different collision partners. Third body collision efficiencies for HNO (+M) for M = Ar, He, N_2, H_2, and NH_3, were calculated using a trajectory-based approach [77]. Briefly, interaction potential energy surfaces for each bath were developed using an automated [78] and validated [79] strategy for permutationally invariant polynomial (PIP) construction [80] and trained using counterpoise corrected MP2/CBS energies and two-point cc-pVTZ and cc-pVQZ complete basis set (CBS) extrapolations. The PIP expansions were used to run ensembles of classical trajectories to compute $\langle \Delta E_d \rangle_M$, the average energy transferred in deactivating collisions [81], and to obtain Lennard-Jones collision rates Z_M via the "one dimensional minimization method" [82]. Third body collision efficiencies relative to M = Ar were defined as $Z_M\beta_M/Z_{Ar}\beta_{Ar}$, where β_M is the weak collider correction to the strong collider rate constant for HNO dissociation [83,84]. Following Troe, we calculated $\beta_M = (\langle \Delta E_d \rangle_M/(\langle \Delta E_d \rangle_M + F_E k_B T))^2$. F_E is related to the thermal fraction of the population of HNO above threshold and was computed using experimental molecular constants [82] and the rigid-rotor, harmonic oscillator approximation; the computed values of F_E for HNO varied from 0.8 to 1.4 over the temperature range 300–2500 K. The good accuracy of the present approach involving trajectory-based evaluations of Troe's expression for β_M has been demonstrated in several recent studies. For example, it was shown to predict the results of a detailed two-dimensional master equation [85] with a mean unsigned deviation of just 28% [77], and it was used to predict relative collision efficiencies with similar accuracy for NH_3 (+M) and N_2H_4 (+M) [86], HO_2 (+M) and H_2O_2 (+M) [78], and O_3 (+M) [87].

Table 4 shows the calculated efficiencies for He, N_2, H_2, and NH_3 compared to Ar. The values for the N_2/Ar ratio agrees well with both

Table 4
Calculated third body efficiencies for HNO(+M) relative to M = Ar.

T/K	M = Ar	He	N_2	H_2	NH_3
300	1.00	1.23	1.83	3.20	5.35
600	1.00	1.37	1.65	3.12	5.82
1000	1.00	1.67	1.73	3.07	6.18
1500	1.00	1.60	1.52	2.58	5.87
2000	1.00	1.53	1.54	2.40	5.73
2500	1.00	1.70	1.55	2.23	5.90

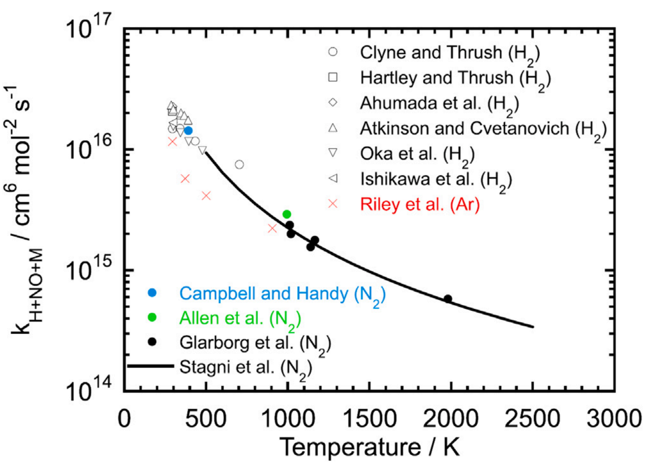

Fig. 5. Arrhenius plot for the reaction H + NO + M → HNO + M (R17). The symbols denote measured values, while the solid line denotes the theoretical low-pressure limit in N_2 by Stagni et al. [25], reversed from k_{17b} through the equilibrium constant. Experimental data are shown for different collision partners: H_2 (Clyne and Thrush [64,65], Hartley and Thrush [66], Ahumada et al. [68], Atkinson and Cvetanovich [69], Oka et al. [70,71], Ishikawa et al. [72]), Ar (Riley et al. [74]), and N_2 (Campbell and Handy [73], Allen et al. [75], Glarborg et al. [76]).

the low temperature experiments and with the recent value calculated by Jasper [81]. The calculated efficiency of H_2 is slightly higher than inferred from experiment, while no comparisons are available for NH_3 and He.

Stagni et al. calculated the rate constant for HNO dissociation in N_2 over a wide range of temperature and pressure. We converted their values for R17b through the equilibrium constant to obtain values for the low and high pressure limits for H + NO (+N_2). Fig. 5 compares the low-pressure limit for R17 with reported experimental results. The resulting rate constant is in excellent agreement with the previous results for H + NO (+N_2) from Campbell and Handy [73], Allen et al. [75], and Glarborg et al. [76]. We note that while the results of Riley et al. [74] for H + NO + Ar are consistent with the other experimental studies within the combined experimental uncertainty, the temperature dependence appears to differ from that of N_2. However, the values calculated by Jasper [81] and in the present work for N_2 compared to Ar indicate values of 1.5–1.7, fairly constant over temperature in the range 300–2000 K.

4. Detailed chemical kinetic model

The chemical kinetic model, including rate coefficients and thermodynamic data, was drawn mainly from the review of nitrogen chemistry by Glarborg et al. [9], but with modifications based on more recent work [28,29]. These included updates of both the H_2-O_2 subset according to recent theoretical work (chemically termolecular reactions H + O_2 + R [88]; H + O_2 (+M) [89]; HO_2 + HO_2 [90]) and the amine subset (NH_3 + HO_2 [25], NH_3 + NH_2 [91], NH_2 + O [92], NH_2 + HO_2 [86,92], HNO + O_2 [93], and subsets for NH_3 pyrolysis [86,94,95], NH_3/NO_2 interactions [28], and H_2NO [96]).

Selected reactions are listed in Table 5, with their rate coefficients and the appropriate references. The reactions that control the ammonia oxidation rate are the chain branching and terminating steps. As discussed above, the chemistry of HNO is of particular interest under the present conditions. The rate constants for HNO + NH_2 (R23) and HNO (+M) (R17) are discussed in the theory section. For HNO + O_2, we rely on the theoretical study by Wang et al. [97]. Reactions of HNO with the O/H radical pool are all fast, but only HNO + H has been characterized over a wider temperature range [92].

Also the H_2NO subset is important, particularly at elevated oxygen concentrations. The rate constant for thermal dissociation of H_2NO (R24b) was drawn from the theoretical work of Klippenstein et al. [92], while values for H_2NO reacting with HO_2, O_2, NH_2, and NO_2 were calculated by Stagni and Cavallotti [96]. The rate constants for H_2NO + O_2 (R25) and H_2NO + NH_2 (R26) are significantly faster than previous estimates, while the value for H_2NO + NO_2 agrees within a factor of 2 with the recent estimate by Glarborg [28] from a study on NH_3/NO_2 interactions.

5. Results and discussion

Ammonia oxidation experiments have been carried out with initial mole fractions of NH_3, O_2, and H_2O of 850 ± 40 ppm, 1–10 ± 0.1%, and 0 or 2.2 ± 0.2%, respectively. Ammonia was highly diluted to limit the heat of reaction. In the present setup, the oxidation rate could only be measured reliably in a narrow temperature range, and all experiments were carried out at temperatures of 1280 ± 16 K.

The reactor was designed to obtain a good approximation to plug-flow in the laminar flow regime. Simulations of the flow reactor experiments were conducted with the Chemkin-PRO software, assuming isothermal plug-flow conditions. The initiation of the reaction may have been affected by the presence of a mixing zone at the entrance of the reactor, by reaction prior to isothermal conditions and/or by surface reactions. Following the analysis of CO/H_2 oxidation in a turbulent flow reactor by Yetter and coworkers [106], the problem of not knowing the induction time was overcome by shifting the calculated data to match the experimental results at a reference point during the consumption of the major reactant (NH_3).

5.1. NH_3 oxidation rate

Fig. 6 compares the measured concentration profiles for NH_3 from the present experiments with modeling predictions for O_2 concentrations in the range 1%–10%. The data at different O_2 levels are not directly comparable, since the reaction temperature had to vary for different oxygen concentrations to obtain useful data. However, the results show that the NH_3 oxidation rate increases with [O_2]. At 1% O_2, the NH_3 profile shows some curvature and possibly the steady-state oxidation rate was not achieved.

The modeling results are in reasonable agreement with the experimental data. The time shift for the four conditions was in the range 30–80 ms. The model overpredicts the oxidation rate at 1% O_2, while at 10% O_2 it is slightly underpredicted. This is illustrated more clearly in Fig. 7, which compares the gradients $d(X_{NH3}/X_{NH3i})/dt$, where X_{NH3i} is the initial mole fraction of NH_3. The non-monotonous curve is caused by the variation in temperature, decreasing from 1296 K (1%–2% O_2) to 1280 K (4% O_2) and 1264 K (10% O_2).

The effect of adding water vapor is investigated for a single condition (4% O_2, Fig. 7). The presence of H_2O has a small inhibiting impact on the reaction. Contrary to the experimental observation, the model predicts that the ammonia oxidation is slightly promoted by the presence of water vapor, indicating that the effect of water is not accurately captured by the kinetic mechanism.

The impact of varying O_2 and H_2O is further investigated in Fig. 8, which compares experimental data from Dean et al. [39] with modeling predictions. Dean et al. conducted their experiments in a type I reactor

Table 5
Selected reactions in the NH_3 oxidation subset. Parameters for use in the modified Arrhenius expression $k = AT^{\beta}\exp(-E/[RT])$. Units are mol, cm, s, cal.

		A	β	E	Source
1.	$NH_2 + H \rightleftarrows NH + H_2$	5.1E08	1.500	3 700	[95]
2.	$NH_2 + O \rightleftarrows HNO + H$	2.8E13	−0.065	−188	[92]
3.	$NH_2 + O \rightleftarrows NH + OH$	3.1E03	2.840	−2 780	[92]
4.	$NH_2 + O \rightleftarrows NO + H_2$	2.4E12	0.112	−347	[92]
5.	$NH_2 + OH \rightleftarrows NH + H_2O$	3.3E06	1.949	−217	[9,98]
6.	$NH_2 + HO_2 \rightleftarrows NH_3 + O_2$	6.0E18	−1.914	306	[99],[a]
		5.9E07	1.592	−1 373	
7.	$NH_2 + HO_2 \rightleftarrows H_2NO + OH$	1.0E12	0.166	−938	[99]
8.	$NH_2 + HO_2 \rightleftarrows HNO + H_2O$	2.2E09	0.791	−1 428	[99]
9.	$NH_2 + O_2 \rightleftarrows H_2NO + O$	2.6E11	0.487	29 050	[100]
10.	$NH_2 + O_2 \rightleftarrows HNO + OH$	2.9E−2	3.764	18 185	[100]
11.	$NH_2 + NO \rightleftarrows NNH + OH$	4.3E10	0.294	−866	[101]
12.	$NH_2 + NO \rightleftarrows N_2 + H_2O$	2.6E19	−2.369	870	[101]
13.	$NH_2 + NO_2 \rightleftarrows H_2NO + NO$	1.1E12	0.110	−1 186	[28],[a]
		−4.3E17	−1.874	588	
14.	$NH_2 + NO_2 \rightleftarrows N_2O + H_2O$	4.3E17	−1.874	588	[28]
15.	$NH + O_2 \rightleftarrows NO + OH$	4.5E08	0.790	1 200	[102]
16.	$NH + O_2 \rightleftarrows HNO + O$	2.1E13	0.000	15 800	[102]
17.	$NO + H(+M) \rightleftarrows HNO(+M)$	3.0E19	−2.165	0	[25], pw
	Low pressure limit	3.9E21	−2.062	0	
	Collision efficiencies N_2 = 1.0, Ar = 0.63, NH_3 = 4, H_2O = 4				
18.	$HNO + H \rightleftarrows NO + H_2$	1.7E10	1.180	−446	[92]
19.	$HNO + O \rightleftarrows NO + OH$	2.3E13	0.000	0	[103]
20.	$HNO + OH \rightleftarrows NO + H_2O$	3.0E13	0.000	0	[104]
21.	$HNO + HO_2 \rightleftarrows HNO_2 + OH$	2.0E03	2.360	8 980	[105]
22.	$HNO + O_2 \rightleftarrows NO + HO_2$	4.0E05	2.300	14 605	[97]
23.	$HNO + NH_2 \rightleftarrows NH_3 + NO$	8.8E06	2.000	−1 555	pw
		6.7E16	−1.407	5	
24.	$HNO + H(+M) \rightleftarrows H_2NO(+M)$	1.9E21	−2.507	4 305	[92], pw
	Low pressure limit	6.1E28	−3.805	4 308	
	Collision efficiencies N_2 = 1.0, NH_3 = 5, H_2O = 12				
25.	$H_2NO + O_2 \rightleftarrows HNO + HO_2$	1.7E05	2.190	18 010	[96]
26.	$H_2NO + NH_2 \rightleftarrows HNO + NH_3$	9.4E12	−0.080	−1 644	[96]

[a] Duplicate reaction: the resulting rate constant is the sum of the two expressions.

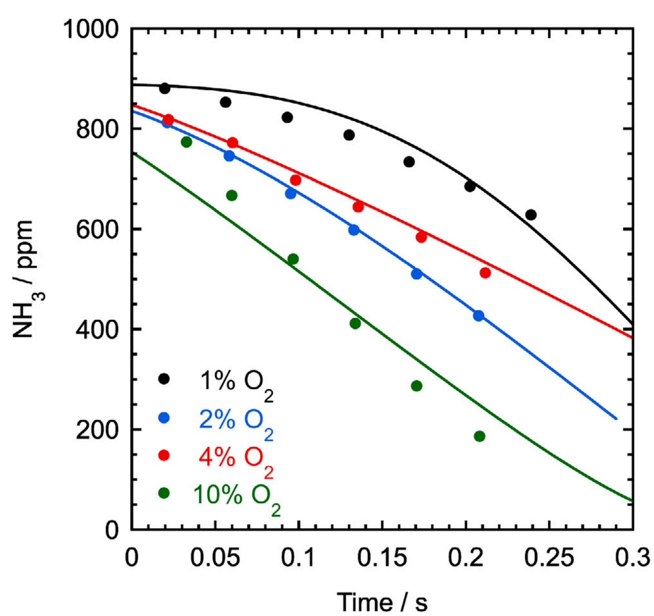

Fig. 6. NH_3 conversion profile in oxidation of 890 ppm ammonia at 1%, 2%, 4%, and 10% O_2, respectively. Symbols denote experimental data and curves denote modeling results. The modeling predictions are shifted in time to match the experimental data at a reference point. Conditions: NH_3 = 890 ppm, O_2 = 1% (1296 K), 2% (1296 K), 4% (1280 K) or 10% (1264 K), H_2O = trace, balance N_2; atm. pressure.

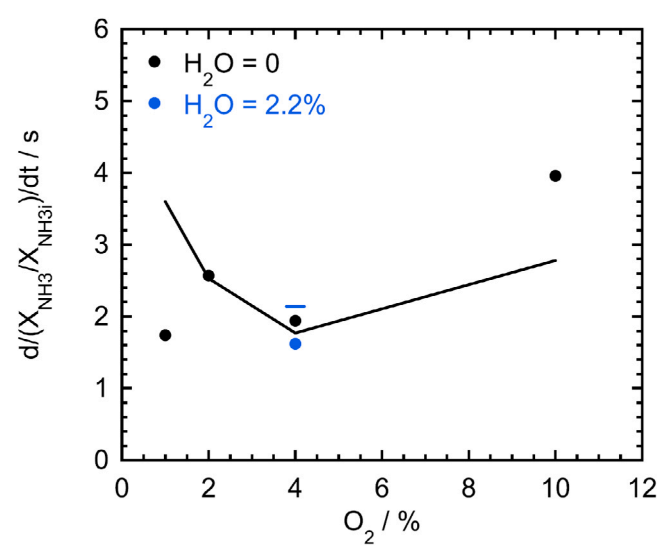

Fig. 7. Comparison of the experimental data from the present work with modeling predictions for oxidation of NH_3 in a quartz flow reactor: effect of O_2 mole fraction on the NH_3 oxidation rate. Solid symbols denote experimental data, while the solid line and the open symbol denote modeling predictions. Conditions: NH_3 = 890 ppm, O_2 = 1% (1296 K), 2% (1296 K), 4% (1280 K) or 10% (1264 K), H_2O = trace (or 2.2%), balance N_2; atm. pressure.

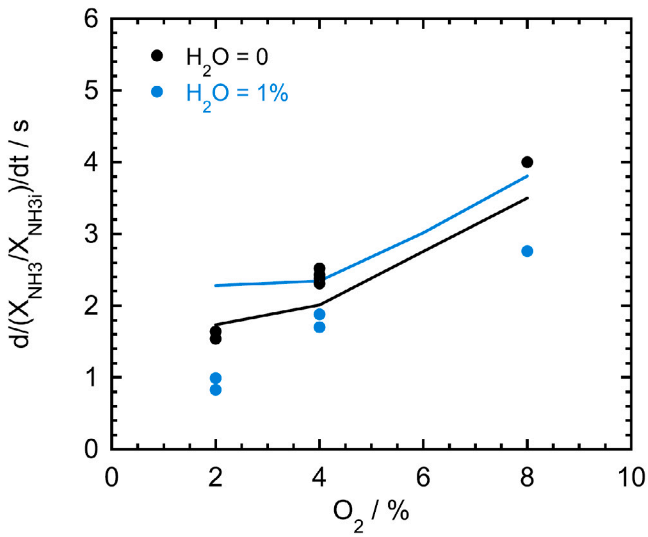

Fig. 8. Comparison of the experimental data from Dean et al. [39] with modeling predictions for oxidation of NH_3 in a quartz flow reactor: effect of O_2 mole fraction and H_2O addition. Symbols denote experimental data, while solid lines denote modeling predictions. NH_3 = 900 ppm, O_2 varying, H_2O = trace or 1%, balance He; temperature 1279 K, pressure is 1.18 atm.

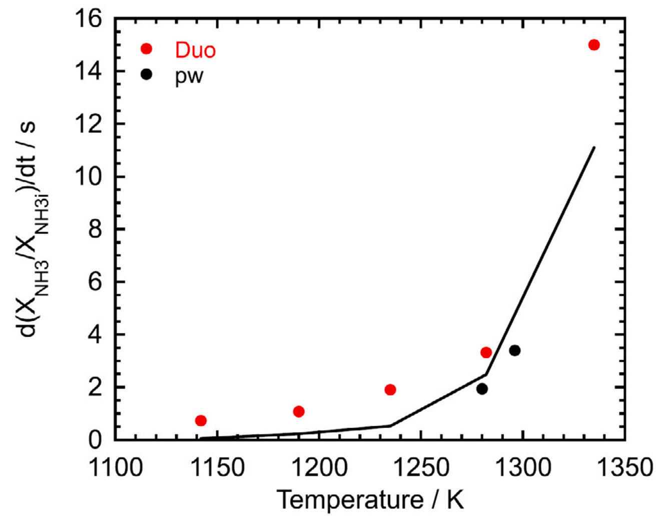

Fig. 9. Comparison of the experimental data of Duo [41] and from the present work with modeling predictions for oxidation of NH_3 at approximately 4% O_2 as a function of temperature. Symbols denote experimental data, while solid lines denote modeling predictions. Conditions: Duo (NH_3 = $9.1\cdot10^{-6}$ mol/l, O_2 = $4.37\cdot10^{-4}$ mol/l, H_2O = trace, balance N_2; atm. pressure); present work (NH_3 = 890 ppm, O_2 = 4%, H_2O = trace, balance N_2; atm. pressure).

(premixed), varying reactor size and flow rate to obtain data at different residence times. Their experiments were carried out with inlet NH_3 and O_2 levels similar to those of the present work, but at slightly higher pressure and with He as inert gas. The experimental approach of Dean et al. allowed reliable oxidation rates to be obtained at 1279 K for O_2 levels of 2%–8%.

The results are in good agreement with those obtained in the present work. The ammonia oxidation rate increases with [O_2], and again addition of water vapor causes a slight inhibition of the reaction. The model predicts well the oxidation rate under dry conditions. However, similarly to what was seen in Fig. 7, the model does not capture well the impact of H_2O.

Duo [41] investigated the NH_3 oxidation under dry conditions as a function of time over a wider temperature range (1140–1340 K) in type II (non-premixed) reactors of varying size. He maintained a constant inlet concentration of the reactants, modifying the inlet mole fractions for each temperature. His results are compared with modeling predictions in Fig. 9. The conditions for the 1282 K experiment are comparable to the present experiments at 4% O_2, which are also shown in the figure. From this and the previous figures, it is clear that the present experimental data and those from Dean et al. and Duo are all essentially in agreement, despite different experimental approaches and slightly different reaction conditions.

As expected, the oxidation rate of NH_3 increases strongly with temperature. The results obtained at temperatures outside the 1280 ± 20 K range have a larger uncertainty due to low or high oxidation rates, respectively. The model captures well the trends observed in the experiment and the difference is probably within the experimental uncertainty.

Fig. 10 shows a reaction path diagram for oxidation of NH_3 under the present conditions. Ammonia is converted to NH_2 by reaction with the O/H radical pool. The amino radical reacts through three major pathways: recycling to NH_3 by H-abstraction reactions with HO_2 (R6), H_2NO (R26), and HNO (R23); oxidation to NO via H_2NO and HNO by reaction with O_2 (R9) and O (R2); or reaction with NO to form N_2 directly (R12) or via NNH (R11).

H_2NO is converted through the sequence $H_2NO \longrightarrow HNO \longrightarrow NO$. The fate of H_2NO and HNO has a significant impact on the overall oxidation rate. Thermal dissociation,

$$H_2NO(+M) \rightleftharpoons HNO + H(+M) \tag{R24b}$$

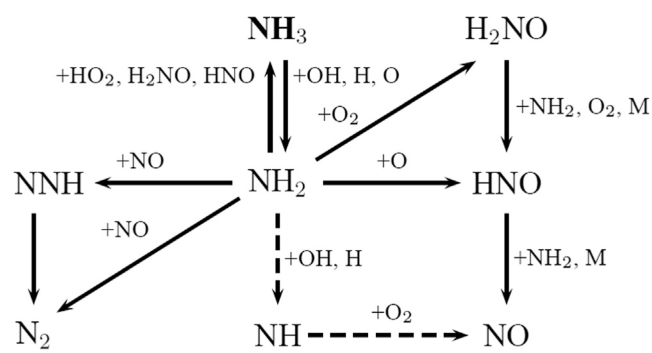

Fig. 10. Reaction path diagram for oxidation of NH_3. The dashed lines show pathways facilitated by presence of H_2O.

$$HNO(+M) \rightleftharpoons H + NO(+M) \tag{R17b}$$

yields atomic hydrogen and promotes oxidation, while reactions with NH_2,

$$H_2NO + NH_2 \rightleftharpoons HNO + NH_3 \tag{R26}$$

$$HNO + NH_2 \rightleftharpoons NO + NH_3 \tag{R23}$$

are chain terminating. The reactions of H_2NO and HNO with O_2 form significant amounts of HO_2,

$$H_2NO + O_2 \rightleftarrows HNO + HO_2 \tag{R25}$$

$$HNO + O_2 \rightleftarrows NO + HO_2, \tag{R22}$$

which subsequently reacts mainly with NH_2 in the terminating step,

$$NH_2 + HO_2 \leftrightarrows NH_3 + O_2 \tag{R6}$$

The loss of NH_2 in (R6) causes this reaction sequence to be overall inhibiting, even though (R25) slightly promotes oxidation.

In the presence of H_2O, atomic oxygen is partly converted to OH through O + H_2O $\rightleftarrows$ OH + OH. The increased OH concentration

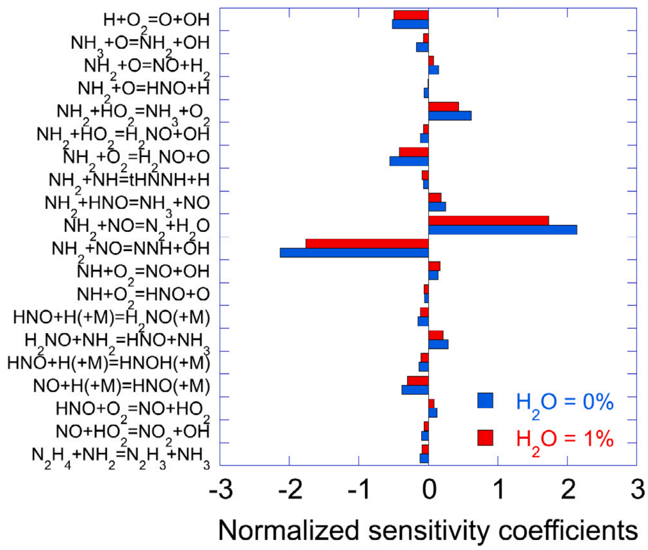

Fig. 11. Sensitivity analysis for the NH_3 mole fraction at 4% O_2 and 1279 K, with 0% and 1% H_2O, respectively (same conditions as in Fig. 8).

facilitates formation of NH through the reaction NH_2 + OH ⇄ NH + H_2O (R5). The NH radical is largely oxidized to NO by reaction with O_2.

A sensitivity analysis with respect to ammonia, eliminating the initiation period by introducing reactive species (radicals, NO, H_2) in the starting composition, is presented in Fig. 11. The predicted oxidation rate of NH_3 results from a delicate balance between chain branching and terminating steps. Even though the nitric oxide concentration is only about 5–15 ppm (see Fig. 12 below), NH_2 is mostly consumed by the fast reaction with NO, yielding NNH + OH (R11) and N_2 + H_2O (R12). The NH_2 + NO reaction exhibits the largest sensitivity coefficients due to its competition between branching (R11) and termination (R12). The branching ratio for NH_2 + NO has been studied extensively [9], but even the small remaining uncertainty has implications for modeling predictions.

The enhancing effect of O_2 on the oxidation rate of NH_3 is mainly due to the chain branching H + O_2 ⇄ O + OH, and, to a lesser extent, NH_2 + O_2 ⇄ H_2NO + OH (R9). Also steps that form atomic hydrogen, i.e., dissociation of HNO (R17b) and H_2NO (R24b), act to promote oxidation. Reaction is inhibited mainly by the chain terminating steps involving NH_2, i.e., NH_2 + O (R4), NH_2 + HO_2 (R6), HNO + NH_2 (R23), and H_2NO + NH_2 (R26). The recent theoretical work on these steps by the groups of Klippenstein and Cavallotti ([25,92,96,99], present work) has been crucial in improving the predictive capability of the model for the present conditions.

5.2. Formation of NO and N_2O

In addition to the NH_3 oxidation rate (discussed above) and flame speed and ignition delay data (see Supplementary Material), it is of interest to evaluate the ability of the model to predict NO and N_2O. Fig. 12 compares the measured concentration profiles for NO from the present experiments and those of Dean et al. with modeling predictions. Nitric oxide is formed rapidly early in the reaction and then reaches a stage where it is in steady-state or increases only slowly. The observed pseudo-steady-state level of NO increases strongly with the O_2 concentration, from approximately 1 ppm at 1% O_2 to more than 20 ppm at 10% O_2. Presence of 1% H_2O is seen to slightly inhibit the NO formation. Where comparable (4% O_2, dry conditions), the present results for NO are in good agreement with those of Dean et al.

The modeling predictions generally capture the NO measurements satisfactorily. The early NO formation may be affected by mixing

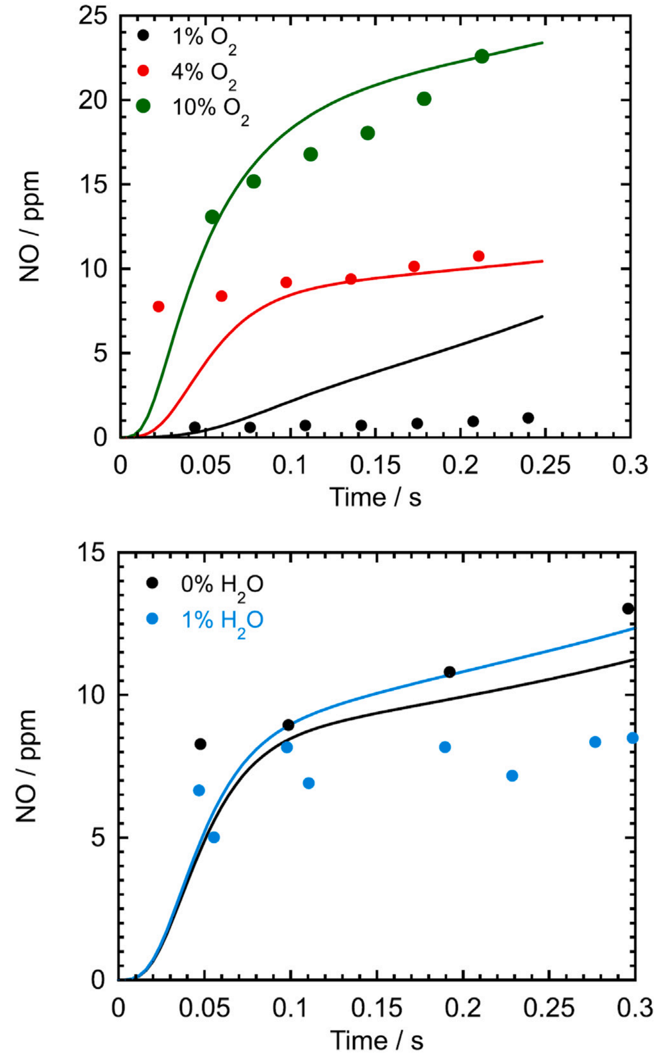

Fig. 12. Comparison of the experimental data from the present work (upper figure) and Dean et al. [39] (lower figure) with modeling predictions for formation of NO. Symbols denote experimental data, while solid lines denote modeling predictions. Present work: conditions as in Fig. 6, with NH_3 = 890 ppm and O_2 = 1%, 4%, and 10% (H_2O = trace). Dean et al.: NH_3 = 900 ppm, O_2 = 4%, H_2O = trace or 1%, balance He; temperature 1279 K, pressure 1.18 atm. The modeling predictions were not shifted in time, unlike those for NH_3.

and/or surface initiation and may not be useful for model comparison. However, the pseudo-steady-state levels of NO and the concentration gradients are predicted well, except at 1% O_2 where the formation rate is strongly overpredicted. Also, presence of water vapor is predicted to slightly promote NO, contrary to observation. These discrepancies are presumably associated with the overprediction of the NH_3 consumption rate (Figs. 7 and 8). Overprediction of the generation of chain carriers leads to overprediction of both the oxidation rate and the NO formation.

Being a strong greenhouse gas, formation of N_2O is a major concern in combustion of NH_3. The two major reactions that form N_2O are [9, 28],

$$NH + NO \rightleftarrows N_2O + H$$

$$NH_2 + NO_2 \rightleftarrows N_2O + H_2O \qquad \text{(R14)}$$

In the flame zone, N_2O is formed mainly by the NH + NO reaction. This high temperature formation is presumably not a large concern,

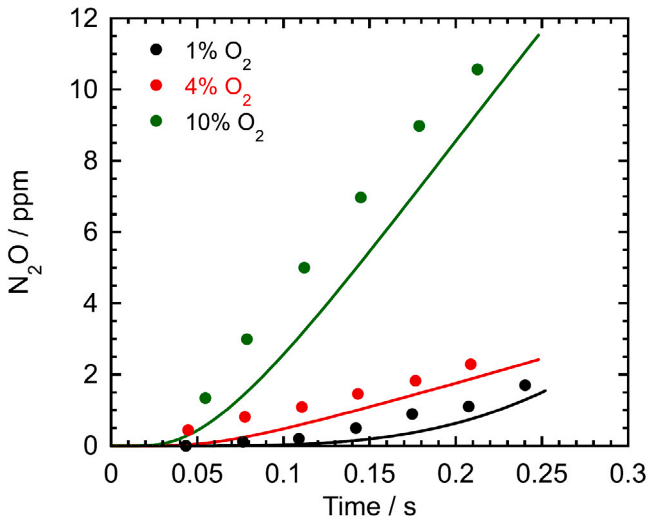

Fig. 13. Comparison of experimental data from the present work with modeling predictions for formation of N_2O. Symbols denote experimental data, while solid lines denote modeling predictions. Conditions as in Fig. 6, with NH_3 = 890 ppm and O_2 = 1%, 4%, and 10% (H_2O = trace). The modeling predictions were not shifted in time, unlike those for NH_3.

because N_2O is rapidly consumed by thermal dissociation or reaction with atomic H. However, N_2O formed at lower temperatures by the NH_2 + NO_2 reaction will only decompose slowly and has a high probability of being emitted.

Fig. 13 compares measured concentration profiles for N_2O from the present experiments with modeling predictions. Most of the N_2O is formed in the region where NO has reached a pseudo-steady-state. The N_2O level increases strongly with the O_2 concentration, from about 2 ppm at 1% to above 10 ppm at 10% O_2. The modeling predictions are in good agreement with the experimental data. At 4%–10% O_2, N_2O is formed mainly by the NH_2 + NO_2 reaction. The NO to NO_2 conversion occurs through NO + HO_2 $\rightleftarrows$ NO_2 + OH and is promoted at high O_2 levels. At 1% O_2, the NO_2 formation is quite limited; here the NH + NO reaction is responsible for most of the N_2O formed. Since these are minor pathways, they are not depicted in Fig. 10.

Concluding remarks

Based on the present work, some important points can be made:

- Under very lean conditions, surface initiation shortens the induction time for NH_3 oxidation in laminar flow quartz reactors. To eliminate this uncertainty, it is important to obtain time or spatially resolved data.
- The post-initiation steady-state NH_3 oxidation rates constitute important data for model validation, along with ignition delays and laminar flame speeds. The present data and the results reported by Dean et al. [39] and Duo [41], which are essentially in agreement despite differences in reactor configuration, serve to characterize the oxidation rate over a significant range of [O_2], [H_2O], and temperature.
- High-level theory was used to calculate the rate constant for HNO + NH_2, indicating that this step is significantly faster than values used in literature. Furthermore, a trajectory based approach was used to determine collision efficiencies for selected bath gases in HNO + M. These results, along with recent theoretical work on NH_2 + O [92], NH_2 + HO_2 [25,99], and H_2NO + NH_2 [96], have been crucial in improving the predictive capability of the model for the present conditions.
- The model generally predicts well the NH_3 oxidation rate as well as the formation of NO and N_2O. However, there are discrepancies at low O_2, and the effect of H_2O is not captured accurately. It is noteworthy that the formation rate of both NO and N_2O increases strongly with [O_2].

CRediT authorship contribution statement

Jie Jian: Experimental and modeling work, Writing – original draft. **Hamid Hashemi:** Design research, Revise draft. **Hao Wu:** Design research, Revise draft. **Peter Glarborg:** Design research, Revise draft. **Ahren W. Jasper:** Theoretical calculations, Revise draft. **Stephen J. Klippenstein:** Theoretical calculations, Revise draft.

Declaration of competing interest

The authors declare that they have no known competing financial interests or personal relationships that could have appeared to influence the work reported in this paper.

Acknowledgments

The authors would like to acknowledge support from Innovation Fund Denmark for the AEngine Grand Solutions project and from the European Horizon 2020 program for the Engimmonia project. J.J. acknowledges support from a CSC scholarship and from Technical University of Denmark. A.W.J. and S.J.K. were supported by the U.S. Department of Energy, Office of Basic Energy Sciences, Division of Chemical Sciences, Geosciences, and Biosciences under contract No. DE-AC02-06CH11357 and as part the Argonne-Sandia Consortium on Pressure-Dependent Chemistry under ANL FWP 59044. Computing resources were provided by Bebop, a high-performance computing cluster operated by the Laboratory Computing Resource Center at Argonne National Laboratory. Dr. Yu Zhang is thanked for helpful discussions about reactor design.

Appendix A. Supplementary data

Supplementary material related to this article can be found online at https://doi.org/10.1016/j.combustflame.2024.113325.

References

[1] J.T. Gray, E. Dimitroff, N.T. Meckel, R.D. Quillian, Ammonia Fuel - Engine Compatibility and Combustion, SAE Techn. Pap. 660156, 1966.
[2] C.D. Wood, Alternative Fuels in Diesel Engines – a Review, SAE Techn. Pap. 810248, 1981.
[3] D. Lee, H.H. Song, Development of combustion strategy for the internal combustion engine fueled by ammonia and its operating characteristics, J. Mech. Sci. Technol. 32 (2018) 1905–1925.
[4] A. Valera-Medina, H. Xiao, M. Owen-Jones, W.I.F. David, P.J. Bowen, Ammonia for power, Prog. Energy Combust. Sci. 69 (2018) 63–102.
[5] H. Kobayashi, A. Hayakawa, K.K.A. Somarathne, E.C. Okafor, Science and technology of ammonia combustion, Proc. Combust. Inst. 37 (2019) 109–133.
[6] A. Valera-Medina, F. Amer-Hatem, A. Azad, I. Dedoussi, M.D. Joannon, R. Fernandes, P. Glarborg, H. Hashemi, X. He, S. Mashurk, J. McGowan, C. Mounaim-Rouselle, A. Ortiz-Prado, J. Ortiz-Valera, I. Rossetti, B. Shu, M. Yehia, H. Xiao, M. Costa, A review on ammonia as a potential fuel: from synthesis to economics, Energy Fuels 35 (2021) 6964–7029.
[7] O. Herbinet, P. Bartocci, A.G. Dana, On the use of ammonia as a fuel – A perspective, Fuel Commun. 11 (2022) 100064.
[8] A.M. Elbaz, S. Wang, T.F. Guiberti, W.L. Roberts, Review on the recent advances on ammonia combustion from the fundamentals to the applications, Fuel Commun. 10 (2022) 100053.
[9] P. Glarborg, J. Miller, B. Ruscic, S. Klippenstein, Modeling nitrogen chemistry in combustion, Prog. Energy Combust. Sci. 67 (2018) 31–68.
[10] B. Mei, X. Zhang, S. Ma, M. Cui, H. Guo, Z. Cao, Y. Li, Experimental and kinetic modeling investigation on the laminar flame propagation of ammonia under oxygen enrichment and elevated pressure conditions, Combust. Flame 210 (2019) 236–246.

[11] B. Mei, J. Zhang, X. Shi, Z. Xi, Y. Li, Enhancement of ammonia combustion with partial fuel cracking strategy: Laminar flame propagation and kinetic modeling investigation of $NH_3/H_2/N_2$/air mixtures up to 10 atm, Combust. Flame 231 (2021) 111472.

[12] S. Zhou, B. Cui, W. Yang, H. Tan, J. Wang, H. Dai, L. Li, Z.U. Rahman, X. Wang, S. Deng, X. Wang, An experimental and kinetic modeling study on NH_3/air, NH_3/h_2/air, NH_3/CO/air, and NH_3/CH_4/air premixed laminar flames at elevated temperature, Combust. Flame 248 (2023).

[13] X. Han, Z. Wang, R. Lin, A.A. Konnov, SAFT regimes and laminar burning velocities: A comparative study of $NH_3 + N_2 + O_2$ and $CH_4 + N_2 + O_2$ flames, Energy Fuels 37 (2023) 7958–7972.

[14] B. Shu, S.K. Vallabhuni, X. He, G. Issayev, K. Moshammer, A. Farooq, R.X. Fernandes, A shock tube and modeling study on the autoignition properties of ammonia at intermediate temperatures, Proc. Combust. Inst. 37 (2019) 205–211.

[15] D. Zhu, Z. Qu, M. Li, S. Agarwal, R. Fernandes, B. Shu, Investigation on the NO formation of ammonia oxidation in a shock tube applying tunable diode laser absorption spectroscopy, Combust. Flame 246 (2022) 112389.

[16] S. Zhu, Q. Xu, R. Tang, J. Gao, Z. Wang, J. Pan, D. Zhang, A comparative study of oxidation of pure ammonia and ammonia/dimethyl ether mixtures in a jet-stirred reactor using SVUV-PIMS, Combust. Flame 250 (2023) 112643.

[17] D. Zhu, L. Ruwe, S. Schmitt, B. Shu, K. Kohse-Hoinghaus, A. Lucassen, Interactions in ammonia and hydrogen oxidation examined in a flow reactor and a shock tube, J. Phys. Chem. A 127 (2023) 2351–2366.

[18] X. He, M. Li, B. Shu, R. Fernandes, K. Moshammer, Exploring the effect of different reactivity promoters on the oxidation of ammonia in a jet-stirred reactor, J. Phys. Chem. A 127 (2023) 1923–1940.

[19] S.A. Alturaifi, O. Mathieu, E.L. Petersen, A shock-tube study of NH_3 and NH_3/H_2 oxidation using laser absorption of NH_3 and H_2O, Proc. Combust. Inst. 39 (2023) 233–241.

[20] M. Pochet, V. Dias, B. Moreau, F. Foucher, H. Jeanmart, F. Contino, Experimental and numerical study, under LTC conditions, of ammonia ignition delay with and without hydrogen addition, Proc. Combust. Inst. 37 (2019) 621–629.

[21] M.V. Manna, P. Sabia, R. Ragucci, M. de Joannon, Ammonia oxidation regimes and transitional behaviors in a jet-stirred flow reactor, Combust. Flame 228 (2021) 388–400.

[22] P. Dagaut, On the oxidation of ammonia and mutual sensitization of the oxidation of NO and ammonia: experimental and kinetic modeling, Combust. Sci. Technol. 194 (2022) 117–129.

[23] R. Tang, Q. Xu, J. Pan, J. Gao, Z. Wang, H. Wei, G. Shu, An experimental and modeling study of ammonia oxidation in a jet stirred reactor, Combust. Flame 240 (2022) 112007.

[24] S. Zhou, W. Yang, S. Zheng, S. Yu, H. Tan, B. Cui, J. Wang, S. Deng, X. Wang, An experimental and kinetic modeling study on the low and intermediate temperatures oxidation of NH_3/O_2/Ar, $NH_3/H_2/O_2$/Ar, NH_3/CO/O_2/Ar, and $NH_3/CH_4/O_2$/Ar mixtures in a jet-stirred reactor, Combust. Flame 248 (2023) 112529.

[25] A. Stagni, C. Cavallotti, S. Arunthanayothin, Y. Song, O. Herbinet, F. Battin-Leclerc, T. Faravelli, An experimental, theoretical and kinetic-modeling study of the gas-phase oxidation of ammonia, React. Chem. Eng. 5 (2020) 696–711.

[26] M. Abián, M. Benés, A. de Goñi, B. Muñoz, M.U. Alzueta, Study of the oxidation of ammonia in a flow reactor. Experiments and kinetic modeling simulation, Fuel 300 (2021) 120979.

[27] P. García-Ruiz, M. Uruén, M. Abián, M.U. Alzueta, High pressure ammonia oxidation in a flow reactor, Fuel 348 (2023) 128302.

[28] P. Glarborg, The $NH_3/NO_2/O_2$ system: Constraining key steps in ammonia ignition and N_2O formation, Combust. Flame 257 (2023) 112311.

[29] M.U. Alzueta, I. Salas, H. Hashemi, P. Glarborg, CO assisted NH_3 oxidation, Combust. Flame 257 (2023) 112438.

[30] A. Stagni, S. Arunthanayothin, M. Dehue, O. Herbinet, F. Battin-Leclerc, P. Bréquigny, C. Mounaïm-Rousselle, T. Faravelli, Low-and intermediate-temperature ammonia/hydrogen oxidation in a flow reactor: Experiments and a wide-range kinetic modeling, Chem. Eng. J. (2023) 144577.

[31] K.P. Shrestha, L. Seidel, T. Zeuch, F. Mauss, Detailed kinetic mechanism for the oxidation of ammonia including the formation and reduction of nitrogen oxides, Energy Fuels 32 (2018) 10202–10217.

[32] K.P. Shrestha, C. Lhuillier, A.A. Barbosa, P. Brequigny, F. Contino, C. Mounaïm-Rousselle, L. Seidel, F. Mauss, An experimental and modeling study of ammonia with enriched oxygen content and ammonia/hydrogen laminar flame speed at elevated pressure and temperature, Proc. Combust. Inst. 38 (2021) 2163–2174.

[33] X. Zhang, S.P. Moosakutty, R.P. Rajan, M. Younes, S.M. Sarathy, Combustion chemistry of ammonia/hydrogen mixtures: Jet-stirred reactor measurements and comprehensive kinetic modeling, Combust. Flame 234 (2021) 111653.

[34] F.L. Dryer, F.M. Haas, J. Santner, T.I. Farouk, M. Chaos, Interpreting chemical kinetics from complex reaction-advection-diffusion systems: Modeling of flow reactors and related experiments, Prog. Energy Combust. Sci. 44 (2014) 19–39.

[35] C.N. Hinshelwood, R.E. Burk, The thermal decomposition of ammonia upon various surfaces, J. Chem. Soc. Trans. 127 (1925) 1105–1117.

[36] K.F. Roenigk, K.F. Jensen, Low-pressure CVD of silicon nitride, J. Electrochem. Soc. 134 (1987) 1777–1785.

[37] P. Glarborg, K. Dam-Johansen, J.A. Miller, R.J. Kee, M.E. Coltrin, Modeling the thermal $DeNO_x$ process in flow reactors. Surface effects and nitrous oxide formation, Int. J. Chem. Kinet. 26 (1994) 421–436.

[38] E.R. Stephens, R.N. Pease, Kinetics of the non-catalytic oxidation of ammonia: Flow experiments, J. Am. Chem. Soc. 72 (1950) 1188–1190.

[39] A.M. Dean, J.E. Hardy, R.K. Lyon, Kinetics and mechanism of NH_3 oxidation, Symp. (Int.) Combust. 19 (1982) 97–105.

[40] R.K. Lyon, D.J. Benn, Kinetics of the NO-NH_3-O_2 reaction, Symp. (Int.) Combust. 17 (1979) 601–610.

[41] W. Duo, Kinetic Studies of the Reactions Involved in Selective Non-Catalytic Reduction of Nitric Oxide (Ph.D. thesis), DTU Chemical Engineering, Technical University of Denmark, 1990.

[42] T. Hulgaard, K. Dam-Johansen, Homogeneous nitrous oxide formation and destruction under combustion conditions, AIChE J. 39 (1993) 1342–1354.

[43] V.J. Wargadalam, G. Löffler, F. Winter, H. Hofbauer, Homogeneous formation of NO and N_2O from the oxidation of HCN and NH_3 at 600–1000 °C, Combust. Flame 120 (2000) 465–478.

[44] Y. Song, H. Hashemi, J. Christensen, C. Zou, P. Marshall, P. Glarborg, Ammonia oxidation at high pressure, Fuel 181 (2016) 358–365.

[45] S. Kasaoka, E. Sasaoka, K. Kawakami, Noncatalytic reduction of nitrogen monoxide with ammonia and oxidation of ammonia with oxygen, Nippon Kagaku Kaishi 1 (1979) 138–144.

[46] S. Kasaoka, E. Sasaoka, M. Nagahiro, Non-catalytic reduction of nitrogen monoxide with ammonia and oxidation of ammonia with oxygen under coexistence of hydrogen, Nippon Kagaku Kaishi 5 (1979) 668–674.

[47] S. Kasaoka, E. Sasaoka, M. Ikoma, Effect of addition of carbon monoxide and hydrogen on non-catalytic reduction of nitrogen monoxide with ammonia, Nippon Kagaku Kaishi 4 (1981) 597–604.

[48] W.D. Monnery, K.A. Hawboldt, A.E. Pollock, W.Y. Svrcek, Ammonia pyrolysis and oxidation in the Claus furnace, Ind. Eng. Chem. Res. 40 (2001) 144–151.

[49] P. Kristensen, P. Glarborg, K. Dam-Johansen, Nitrogen chemistry during burnout in fuel-staged combustion, Combust. Flame 107 (1996) 211–222.

[50] A.M. Mebel, E.W.G. Diau, M.-C. Lin, K. Morokuma, Theoretical rate constants for the $NH_3 + NO_x \rightarrow NH_2 + HNO_x$ (x = 1, 2) reactions by ab initio MO/VTST calculations, J. Phys. Chem. 100 (1996) 7517–7525.

[51] S. Xu, M.C. Lin, Ab initio chemical kinetics for the $NH_2 + HNO_x$ reactions, part I: Kinetics and mechanism for NH_2 + HNO, Int. J. Chem. Kin. 41 (2009) 667–677.

[52] T.R. Roose, R.K. Hanson, C.H. Kruger, Decomposition of NO in the presence of NH_3, Shock Tube Shock Wave Res. (1978) 245–253.

[53] T.R. Roose, R.K. Hanson, C.H. Kruger, A shock tube study of the decomposition of NO in the presence of NH_3, Symp. (Int.) Combust. 18 (1981) 853–862.

[54] S.J. Klippenstein, L.B. Harding, B. Ruscic, Ab initio computations and active thermochemical tables hand in hand: Heats of formation of core combustion species, J. Phys. Chem. A 121 (2017) 6580–6602.

[55] S.J. Klippenstein, Variational optimizations in RRKM theory calculations for unimolecular dissociations with no reverse barrier, J. Chem. Phys. 96 (1992) 367–371.

[56] H. Werner, P. Knowles, G. Knizia, F. Manby, M. Schütz, P. Celani, W. Györffy, D. Kats, T. Korona, R. Lindh, MOLPRO, 2012.1, a package of ab initio programs, 2012, See http://www.molpro.net.

[57] J.F. Stanton, J. Gauss, L. Cheng, M.E. Harding, D.A. Matthews, P.G. Szalay, A.A. Auer, CFOUR, coupled-cluster techniques for computational chemistry, a quantum-chemical program package, 2019, With contributions from A. A. Auer, R. J. Bartlett, U. Benedikt, C. Berger, D. E. Bernholdt, Y. J. Bomble, O. Christiansen, F. Engel, R. Faber, M. Heckert, O. Heun, M. Hilgenberg, C. Huber. For the current version, see: http://www.cfour.de.

[58] M. Kállay, P.R. Surján, Higher excitations in coupled-cluster theory, J. Chem. Phys. 115 (2001) 2945–2954.

[59] M. Kállay, MRCC, a String-Based Quantum Chemical Program Suite, Budapest University of Technology and Economics, Budapest, Hungary, 2001.

[60] M.J. Frisch, G. Trucks, H.B. Schlegel, G.E. Scuseria, M.A. Robb, J.R. Cheeseman, G. Scalmani, V. Barone, G.A. Petersson, H. Nakatsuji, X. Li, M. Caricato, A.V. Marenich, J. Bloino, B.G. Janesko, R. Gomperts, B. Mennucci, H.P. Hratchian, J.V. Ortiz, A.F. Izmaylov, J.L. Sonnenberg, Williams, F. Ding, F. Lipparini, F. Egidi, J. Goings, B. Peng, A. Petrone, T. Henderson, D. Ranasinghe, V.G. Zakrzewski, J. Gao, N. Rega, G. Zheng, W. Liang, M. Hada, M. Ehara, K. Toyota, R. Fukuda, J. Hasegawa, M. Ishida, T. Nakajima, Y. Honda, O. Kitao, H. Nakai, T. Vreven, K. Throssell, J.A. Montgomery Jr., J.E. Peralta, F. Ogliaro, M.J. Bearpark, J.J. Heyd, E.N. Brothers, K.N. Kudin, V.N. Staroverov, T.A. Keith, R. Kobayashi, J. Normand, K. Raghavachari, A.P. Rendell, J.C. Burant, S.S. Iyengar, J. Tomasi, M. Cossi, J.M. Millam, M. Klene, C. Adamo, R. Cammi, J.W. Ochterski, R.L. Martin, K. Morokuma, O. Farkas, J.B. Foresman, D.J. Fox, Gaussian 16 Rev. C01, Wallington, CT, USA, 2019.

[61] Y. Georgieskii, L.B. Harding, S.J. Klippenstein, VaReCoF, Argonne National Laboratory, 2011, see https://tcg.cse.anl.gov/papr/codes/varecof.html.

[62] Y. Georgievskii, J.A. Miller, M.P. Burke, S.J. Klippenstein, Reformulation and solution of the master equation for multiple-well chemical reactions, J. Phys. Chem. A 117 (2013) 12146–12154.

[63] Y. Georgieskii, S.J. Klippenstein, MESS 2016.3.23, Argonne National Laboratory, 2016, see https://tcg.cse.anl.gov/papr/codes/mess.html.
[64] M.A.A. Clyne, B.A. Thrush, Reaction of hydrogen atoms with nitric oxide, Trans. Faraday Soc. 57 (1961) 1305–1314.
[65] M.A.A. Clyne, B.A. Thrush, Mechanism of chemiluminescent reactions involving nitric oxide – the H + NO reaction, Discuss. Faraday Soc. 33 (1962) 139–148.
[66] D.B. Hartley, B.A. Thrush, The rates of elementary processes in the chain reaction between hydrogen and oxygen III. Kinetics of the combination of hydrogen atoms with nitric oxide, Proc. R. Soc. Lond. Ser. A Math. Phys. Eng. Sci. 297 (1967) 520–533.
[67] T. Hikida, J.A. Eyre, L.M. Dorfman, Pulse radiolysis studies. XX. Kinetics of some addition reactions of gaseous hydrogen atoms by fast lyman-α absorption spectrophotometry, J. Chem. Phys. 54 (1971) 3422–3428.
[68] J.J. Ahumada, J.V. Michael, D.T. Osborne, Pressure dependence and third body effects on the rate constants for H + O_2, H + NO, and H + CO, J. Chem. Phys. 57 (1972) 3736–3745.
[69] R. Atkinson, R.J. Cvetanović, Determination of the rates of hydrogen atom reaction with NO by a modulation technique, Can. J. Chem. 51 (1973) 370–372.
[70] K. Oka, D.L. Singleton, R.J. Cvetanović, Mercury photosensitized reaction of H_2 in the presence of NO. Rate constants of the H + NO + M→ HNO + M and HgH + NO → HNO + Hg reactions, J. Chem. Phys. 66 (1977) 713–721.
[71] K. Oka, D.L. Singleton, R.J. Cvetanović, Temperature dependence of the rate of reaction H + NO + M → HNO + M for M = H_2 and the relative third body efficiencies of NO and H_2, J. Chem. Phys. 67 (1977) 4681–4689.
[72] Y.-i. Ishikawa, K.-i. Sugawara, S. Sato, The rate constants for H and D-atom additions to O_2, NO, acetylene, and 1,3-butadiene, Bull. Chem. Soc. Japan 52 (1979) 3503–3506.
[73] I.M. Campbell, B.J. Handy, Studies of reactions of atoms in a discharge flow stirred reactor. Part 1. The O + H_2 + NO system, J. Chem. Soc. Faraday Trans. 1 71 (1975) 2097–2106.
[74] P.S. Riley, B. Cosic, A. Fontijn, The H + NO recombination reaction over a wide temperature range, Int. J. Chem. Kinet. 35 (2003) 374–380.
[75] M.T. Allen, R.A. Yetter, F.L. Dryer, Hydrogen nitrous oxide kinetics - implications of the N_xH_y species, Combust. Flame 112 (1998) 302–311.
[76] P. Glarborg, M. Østberg, M.U. Alzueta, K. Dam-Johansen, J.A. Miller, The recombination of hydrogen atoms with nitric oxide at high temperatures, Proc. Combust. Inst. 27 (1998) 219–226.
[77] A.W. Jasper, Microcanonical rate constants for unimolecular reactions in the low-pressure limit, J. Phys. Chem. A 124 (2020) 1205–1226.
[78] D.R. Moberg, A.W. Jasper, Permutationally invariant polynomial expansions with unrestricted complexity, J. Chem. Theory Comput. 17 (2021) 5440–5455.
[79] A.W. Jasper, M.J. Davis, Parameterization strategies for intermolecular potentials for predicting trajectory-based collision parameters, J. Phys. Chem. A 123 (2019) 3464–3480.
[80] B.J. Braams, J.M. Bowman, Permutationally invariant potential energy surfaces in high dimensionality, Int. Rev. Phys. Chem. 28 (2009) 577–606.
[81] A.W. Jasper, Predicting third-body collision efficiencies for water and other polyatomic baths, Faraday Discuss. 238 (2022) 68–86.
[82] A.W. Jasper, J.A. Miller, Lennard-jones parameters for combustion and chemical kinetics modeling from full-dimensional intermolecular potentials, Combust. Flame 161 (2014) 101–110.
[83] J. Troe, Theory of thermal unimolecular reactions at low pressures. I. Solutions of the master equation, J. Chem. Phys. 66 (1977) 4745–4757.
[84] D.C. Tardy, B.S. Rabinovitch, Intermolecular vibrational energy transfer in thermal unimolecular systems, Chem. Rev. 77 (1977) 369–408.
[85] A.W. Jasper, K.M. Pelzer, J.A. Miller, E. Kamarchik, L.B. Harding, S.J. Klippenstein, Predictive a priori pressure-dependent kinetics, Science 346 (2014) 1212–1215.
[86] P. Glarborg, H. Hashemi, S. Cheskis, A.W. Jasper, On the rate constant for NH_2 + HO_2 and third-body collision efficiencies for NH_2 + H (+ M) and NH_2 + NH_2 (+ M), J. Phys. Chem. A 125 (2021) 1505–1516.
[87] J. Jian, H. Hashemi, H. Wu, A.W. Jasper, P. Glarborg, A reaction mechanism for ozone dissociation and reaction with hydrogen at elevated temperature, Fuel 322 (2022) 124138.
[88] M.P. Burke, S.J. Klippenstein, Ephemeral collision complexes mediate chemically termolecular transformations that affect system chemistry, Nature Chem. 9 (2017) 1078–1082.
[89] L. Lei, M.P. Burke, Mixture rules and falloff are now major uncertainties in experimentally derived rate parameters for H + O_2 (+M) ⇄ HO_2 (+M), Combust. Flame 213 (2020) 467–474.
[90] S.J. Klippenstein, R. Sivaramakrishnan, U. Burke, K.P. Somers, H.J. Curran, L. Cai, H. Pitsch, M. Pelucchi, T. Faravelli, P. Glarborg, HO_2 + HO_2: High level theory and the role of singlet channels, Combust. Flame 243 (2022) 111975.
[91] P. Marshall, P. Glarborg, Probing high-temperature amine chemistry: Is the reaction NH_3 + NH_2 ⇄ N_2H_3 + H_2 important? J. Phys. Chem. A 127 (2023) 2601–2607.
[92] S.J. Klippenstein, C.R. Mulvihill, P. Glarborg, Theoretical kinetics predictions for reactions on the NH_2O potential energy surface, J. Phys. Chem. A 127 (2023) 8650–8662.
[93] J.E. Chavario Cañas, M. Monge-Palacios, X. Zhang, S.M. Sarathy, Probing the gas-phase oxidation of ammonia: Addressing uncertainties with theoretical calculations, Combust. Flame 235 (2022) 111708.
[94] P. Marshall, G. Rawling, P. Glarborg, New reactions of diazene and related species for modelling combustion of amine fuels, Mol. Phys. 119 (2021) e1979674.
[95] P. Glarborg, H. Hashemi, P. Marshall, Challenges in kinetic modeling of ammonia pyrolysis, Fuel Commun. 10 (2022) 100049.
[96] A. Stagni, C. Cavallotti, H-abstractions by O_2, NO_2, NH_2, and HO_2 from H_2NO: Theoretical study and implications for ammonia low-temperature kinetics, Proc. Combust. Inst. 39 (2023) 633–641.
[97] Q.-D. Wang, Y. Sun, H.J. Curran, Comparative chemical kinetic analysis and skeletal mechanism generation for syngas combustion with NO_x chemistry, Energy Fuels 34 (2019) 949–964.
[98] S.J. Klippenstein, L.B. Harding, B. Ruscic, R. Sivaramakrishnan, N.K. Srinivasan, M.-C. Su, J.V. Michael, Thermal decomposition of NH_2OH and subsequent reactions: Ab initio transition state theory and reflected shock tube experiments, J. Phys. Chem. A 113 (2009) 10241–10259.
[99] S.J. Klippenstein, P. Glarborg, Theoretical kinetics predictions for NH_2 + HO_2, Combust. Flame 236 (2022) 111787.
[100] S.J. Klippenstein, L.B. Harding, P. Glarborg, J.A. Miller, The role of NNH in NO formation and control, Combust. Flame 158 (2011) 774–789.
[101] S. Song, R.K. Hanson, C.T. Bowman, D.M. Golden, Shock tube determination of the overall rate of NH_2 + NO → products in the thermal de-NO_x temperature window, Int. J. Chem. Kinet. 33 (2001) 715–721.
[102] H.-J. Römming, H.G. Wagner, A kinetic study of the reactions of NH (X3Σ-) with O_2 and NO in the temperature range from 1200 to 2200 K, Symp. (Int.) Combust. 26 (1996) 559–566.
[103] S. Inomata, N. Washida, Rate constants for the reactions of NH_2 and HNO with atomic oxygen at temperatures between 242 and 473 K, J. Phys. Chem. A 103 (1999) 5023–5031.
[104] F. Sun, J.D. DeSain, G. Scott, P.Y. Hung, R.I. Thompson, G.P. Glass, R.F. Curl, Reactions of NH_2 with NO_2 and of OH with NH_2O, J. Phys. Chem. A 105 (2001) 6121–6128.
[105] S.H. Mousavipour, S.S. Asemani, Theoretical study on the dynamics of the reaction of HNO with HO_2, J. Phys. Chem. A 119 (2015) 5553–5565.
[106] R.A. Yetter, F.L. Dryer, H. Rabitz, Flow reactor studies of carbon monoxide/hydrogen/oxygen kinetics, Combust. Sci. Technol. 79 (1991) 129–140.